Surface-Supported Robust 2D Lanthanide-Carboxylate Coordination Networks

José I. Urgel, Borja Cirera, Yang Wang, Willi Auwärter, Roberto Otero, José M. Gallego, Manuel Alcamí, Svetlana Klyatskaya, Mario Ruben, Fernando Martín, Rodolfo Miranda, David Ecija, and Johannes V. Barth**

Lanthanide-based metal–organic compounds and architectures are promising systems for sensing, heterogeneous catalysis, photoluminescence, and magnetism. Herein, the fabrication of interfacial 2D lanthanide-carboxylate networks is introduced. This study combines low- and variable-temperature scanning tunneling microscopy (STM) and X-ray photoemission spectroscopy (XPS) experiments, and density functional theory (DFT) calculations addressing their design and electronic properties. The bonding of ditopic linear linkers to Gd centers on a Cu(111) surface gives rise to extended nanoporous grids, comprising mononuclear nodes featuring eightfold lateral coordination. XPS and DFT elucidate the nature of the bond, indicating ionic characteristics, which is also manifest in appreciable thermal stability. This study introduces a new generation of robust low-dimensional metallosupramolecular systems incorporating the functionalities of the f-block elements.

1. Introduction

Lanthanides are versatile metallic elements the functional properties of which are exploited in a wide variety of high-technology applications, notably including optical fibers, displays, light emitting diodes, strong magnets, sensors, bioimaging, and medicine.[1–3] Considerable efforts were devoted to explore novel coordination architectures incorporating lanthanides, typically providing high coordination numbers that give rise to unusual topologies in bulk chemistry.[4–11]

J. I. Urgel, Prof. W. Auwärter, Dr. D. Ecija, Prof. J. V. Barth
Physik Department E20
Technische Universität München
85748, Garching, Germany
E-mail: david.ecija@imdea.org; jvb@tum.de

B. Cirera, Dr. Y. Wang, Dr. R. Otero, Dr. J. M. Gallego, Dr. M. Alcamí, Prof. F. Martín, Prof. R. Miranda, Dr. D. Ecija
IMDEA Nanoscience
28049 Madrid, Spain

Dr. Y. Wang, Dr. M. Alcamí, Prof. F. Martín
Departamento de Química Módulo 13
Universidad Autónoma de Madrid
28049 Madrid, Spain

Dr. R. Otero, Prof. R. Miranda
Departamento Física de la Materia Condensada
Universidad Autónoma de Madrid
28049 Madrid, Spain

Dr. J. M. Gallego
Instituto de Ciencia de Materiales de Madrid
CSIC, 28049 Madrid, Spain

Dr. S. Klyatskaya, Prof. M. Ruben
Institute of Nanotechnology
Karlsruhe Institute of Technology
76344 Eggenstein-Leopoldshafen, Germany

Prof. M. Ruben
IPCMS-CNRS UMR 7504
Université de Strasbourg
67034 Strasbourg Cedex 2, France

Prof. F. Martín
Condensed Matter Physics Center
Universidad Autónoma de Madrid
28049 Madrid, Spain

DOI: 10.1002/smll.201502761

Supramolecular chemistry on surfaces has provided a variety of protocols to design low-dimensional nanoarchitectures on surfaces incorporating alkali or d-block metals.[12–33] Recently, we introduced the lanthanide-directed assembly of low-dimensional nanostructures and networks based on a unique fivefold coordination between cerium (or gadolinium) atoms and linker species equipped with carbonitrile termini.[34–36] However, lanthanide-based molecular engineering on surfaces is still in its infancy and further advances are mandatory to fully exploit the potential of rare-earth elements embedded in tailored interfacial nanoarchitectures.

In this work, we present a combined scanning tunneling microscopy (STM), X-ray photoelectron spectroscopy (XPS), and density functional theory (DFT) study of metal–organic arrays created on a pristine copper surface by the coordination of gadolinium with linear ditopic linkers equipped with carboxyl groups (4,1′,4′,1″-terphenyl-1,4″-dicarboxylic acids, TDA, cf. **Figure 1**a and the Supporting Information for synthesis). To date, surface-confined di- and tri-carboxylic acid species have been reported to readily undergo coordination with alkali and d-block transition metals.[14–18,20,23,25,28,37–39] Our results present *f* elements in carboxylate coordinative schemes, showing the formation of a reticular metal–organic assembly based on carboxylate–Gd interactions involving an unprecedented lateral coordination number on surfaces of 8 for the expressed mononuclear Gd nodes. Variable-temperature imaging highlights the robustness of the assemblies up to ≈400 K. Complementary XPS experiments provide space-average insights about the electronic nature of the metal–organic architectures revealing that the coupling motif is based on anionic carboxylate moieties and positively charged Gd centers. DFT simulations clarify the geometric details and bonding distances of the coordination motifs and corroborate ionic characteristics of the lanthanide–carboxylate bond, bearing similarities to surface-confined coordinative schemes comprising alkali metals.[23,25,40,41]

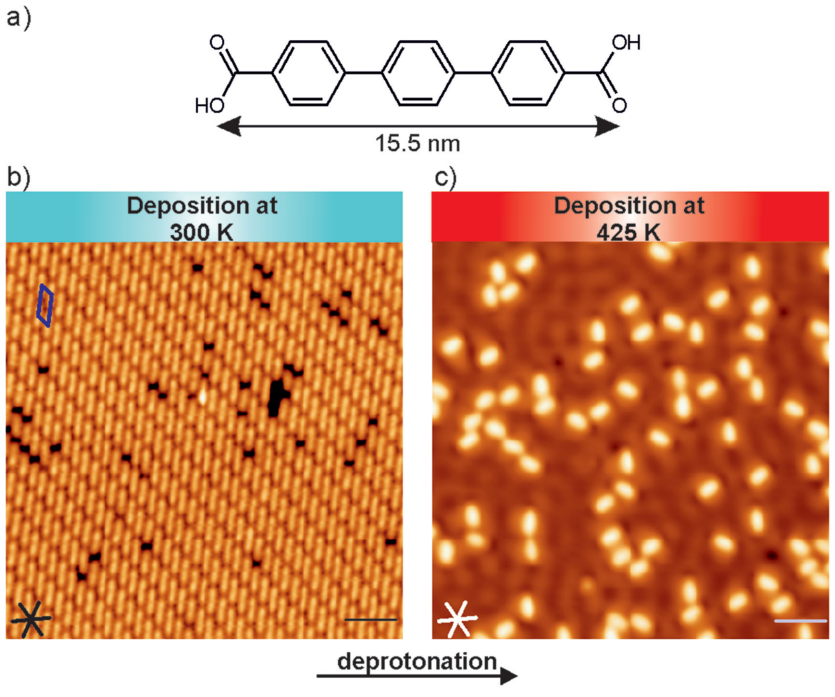

Figure 1. Chemical structure and LT-STM topographs of TDA species deposited at different temperatures on Cu(111). a) Molecular structure of TDA. b) LT-STM image showing the tetragonal supramolecular network stabilized by H-bond interactions ($V_b = -1$ V and $I = 400$ pA). The violet tetragon depicts the unit cell. c) LT-STM image of a submonolayer of TDA reflecting the full deprotonation of the carboxylic groups ($V_b = 0.1$ V and $I = 200$ pA). Scale bars: 3 nm.

2. Results and Discussion

The deposition of TDA on pristine Cu(111) at RT (room temperature) gives rise to close-packed and well-ordered arrays, in which individual molecules are visualized as rods, featuring an oblique lattice, with unit cell vectors of 8.2 ± 0.7 and 18.7 ± 0.7 Å, spanning an angle of 55° (cf. Figure 1b). Thus the molecular species preserve their chemical integrity, are mobile and form networks with a chaining motif that reflects directional H-bonding (cf. Figure SI1, Supporting Information).[42] At slightly higher substrate temperatures (308 K), variable-temperature STM signals almost full deprotonation, which is observed by the appearance of mainly isolated rod-like species, associated with fully deprotonated compounds,[38] coexisting with rarely appearing unaltered TDA islands. Above this substrate temperature, linker endgroups are completely transformed (cf. Figure 1c for low-temperature visualization of the carboxylates), however, in contrast to experiments employing related compounds on copper surfaces, with the TDA species no metal–organic compounds evolve where Cu adatoms are incorporated.[14,43]

In order to assess the affinity of the carboxylate groups to lanthanide elements, gadolinium (Gd) is deposited onto a Cu(111) surface with TDA molecules held at ≈423 K. Following this protocol, **Figure 2**a depicts the formation of extended patches of 2D reticulated supramolecular structures, coexisting with isolated carboxylate species. The best samples were produced at 423 K following adequate annealing periods. The high degree of perfection of coordination motifs in the domains strongly indicates that self-correction processes are operative, suggesting a thermodynamically driven network evolution. High-resolution imaging allows us to discern the network architecture, which features a square unit cell of 19.5 ± 0.7 Å, with a Gd:linker stoichiometry of 1:2 (cf. Figure 2b). Hereby, molecular species are visualized as rods, and Gd centers as voids (cf. Figure 2a,b) or dim protrusions (cf. Figure SI2, Supporting Information) depending on the employed tunneling conditions and tip state. Importantly, there is only a single rare-earth center in the coordination node. More complex nodes such as the previously encountered dinuclear Co or Fe motifs in carboxylate-based metal–organic networks,[44,45] or the recently

DOI: 10.1002/smll.201502761

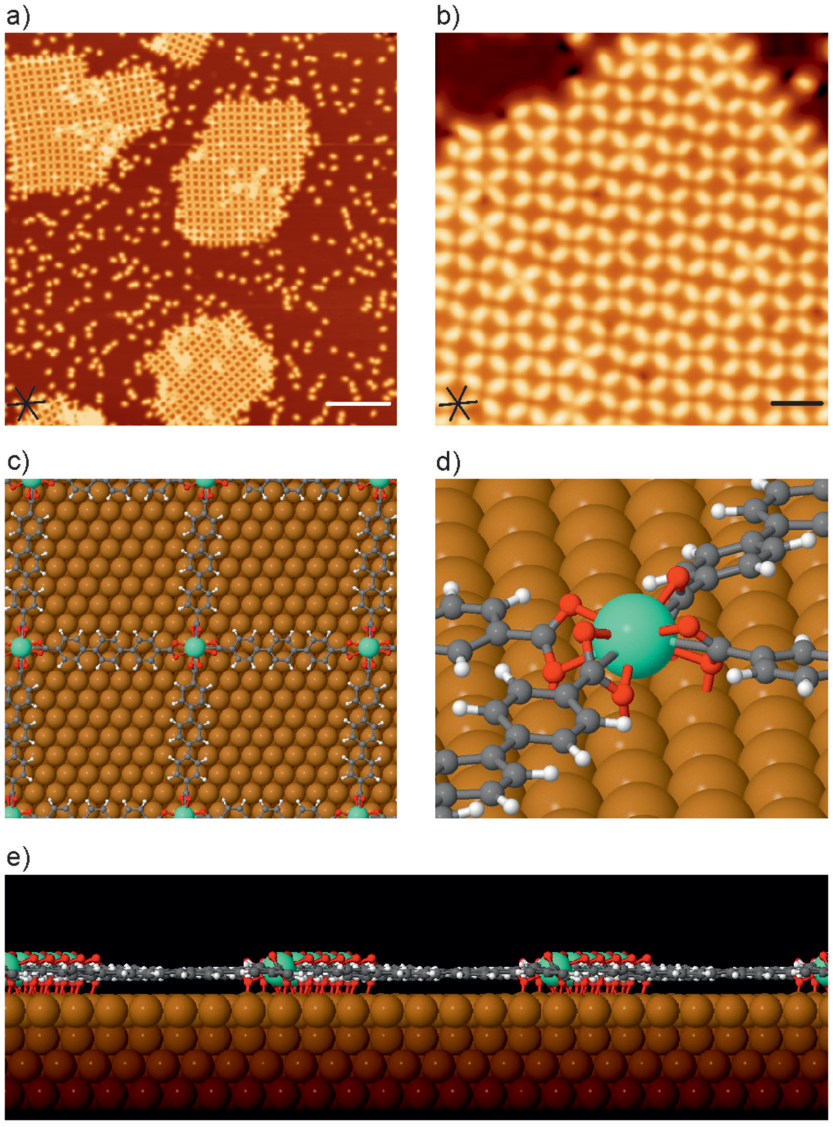

Figure 2. Lanthanide-directed Gd:TDA metallosupramolecular network on Cu(111). a) Long-range topograph (V_b = 1 V and I = 80 pA). Scale bar: 15 nm. b) High-resolution image (V_b = –1 V and I = 300 pA). Scale bar: 3 nm. c–e) DFT optimized geometry of the assembly. c) Top-view. d) Zoom-in perspective view emphasizing the eightfold Gd–O coordination motif. e) Side-view. Gd, C, O, H, and Cu atoms are depicted in green, gray, red, white, and orange, respectively.

suggested di-iron-nodes in upright positions coordinated by pyridil moieties[33] are excluded in the gadolinium-directed fourfold reticulated architecture, because the rare-earth atomic diameter is too large for the nodal space and Cu adatoms did not participate in coordination schemes in the explored range of temperatures. The mononuclear Gd vertex is surrounded by four molecular linkers, reflecting a square-planar coordination motif with four chelating rare-earth-carboxylate bonds and a projected average Gd—O bond length of 2.6 ± 0.7 Å (see below). This coupling scheme resulting in a coordination number of 8 is unprecedented for interfacial metallosupramolecular architectures and hints toward a prevalent ionic character versus covalency in the lanthanide metal–organic bonds, also encountered in bulk chemistry.[1]

To further rationalize the Gd-carboxylate supramolecular network, we performed DFT simulations. Figure 2c–e illustrates an optimized geometry of the assembly, highlighting the eightfold Gd–O lateral coordination and yielding a binding energy of 4.99 eV per molecule (for comparison in the absence of the substrate this binding energy is 3.27 eV per molecule). Molecules are adsorbed with their polyphenylene backbone almost planar. The average interphenylene dihedral angle is 10.9°, i.e., individual rings are oriented approximately ±5° with respect to the surface plane. The planarization of the molecular linkers is similar to that encountered for the surface-confined fivefold metal–organic assemblies based on Ce(Gd) and dicarbonitrile-terphenyl and dicarbonitrile-quarterphenyl species.[34–36]

Remarkably, the Gd presents an adsorption height of 3.1 Å with respect to the surface (cf. Figure 2e). In order to balance Gd–O attractive interactions and intermolecular O···O steric hindrance, the carboxylate termini rotate 44.5° about their sigma bonds, thus allowing the high coordination number of 8, with a Gd–O bond length of 2.4–2.7 Å, in accordance with the experimental geometry and similar values reported for 3D lanthanide–oxygen donor complexes.[46] This eightfold Gd–O lateral coordination motif differs from the coordination nodes in the related nanoporous Fe and Co-terephthalate arrays fabricated on Cu(100) or Au(111), which incorporate four lateral carboxylate bonds to dimetal centers.[44,45] We attribute the distinct coordinative scheme to the larger atomic diameter of the Gd center and the propensity of rare-earth metals toward higher coordination numbers.

Next, the thermal stability of the Gd-TDA assemblies is explored by holding the samples at distinct temperatures during STM-measurements. Continuous imaging at 77 K, RT and at 360 K exhibits stable island edges and identical assemblies to those achieved at 6 K (cf. **Figure 3** and Figure SI3, Supporting Information), highlighting an appreciable thermal robustness, also encountered in surface-confined metal-carboxylate networks involving alkali or d-block centers.[17,25,30,47] Importantly, the variable-temperature imaging shows certain degree of flexibility of the coordination nodes, which could be of relevance for hosting[17] functional guest species. Further inspection at 393 K (the technical limit for the variable-temperature STM) signals the initial steps of desintegration of edges of the assemblies (cf. Figure SI4, Supporting Information). Thus, for surface-confined lanthanide-directed nanostructures, the Gd-TDA grids based on eightfold Gd–O bonds appear more

DOI: 10.1002/smll.201502761

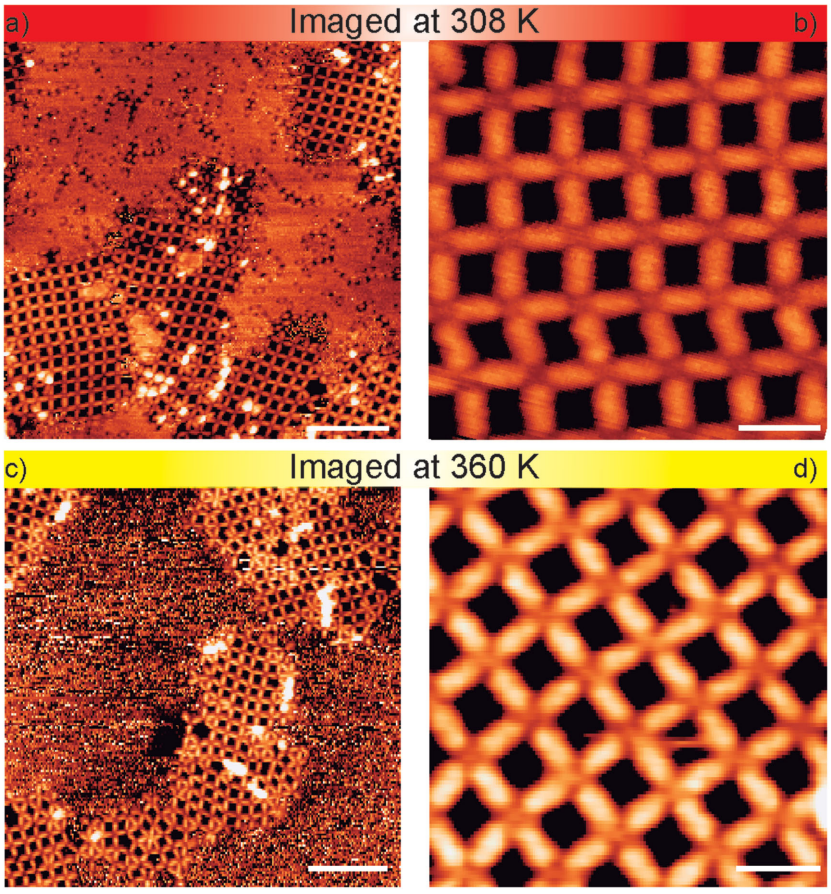

Figure 3. Variable-temperature STM images of the Gd-TDA network assembly on Cu(111) recorded at a,b) 308 K and c,d) 360 K. (a) Long-scale image (V_b = 1.3 V and I = 500 pA, scale bar = 10 nm). (b) High-resolution STM image (V_b = 1.3 V and I = 480 pA, scale bar = 2 nm). (c) Large-range STM image highlighting the stability of the islands at high-temperature (V_b = 1.1 V and I = 370 pA, scale bar = 10 nm). (d) High-resolution STM image (V_b = 1.6 V and I = 400 pA, scale bar = 2 nm).

stable than the recently reported fivefold Ce-carbonitrile networks on Ag(111), which are dissolved at T = 300 K.[34]

Finally, to obtain information of the chemical state of the molecules and Gd atoms, and to get further knowledge of the electronic nature of the Gd–O metal–organic bond, the reticular Gd-carboxylate architectures are inspected by X-ray photoelectron spectroscopy. In **Figure 4**a, the oxygen 1s XPS data are shown for a multilayer of TDA deposited on the surface held at 308 K (upper violet curve), for a TDA submonolayer after annealing to 423 K without Gd (middle green curve), and for a TDA submonolayer after coadsorption of Gd at a surface temperature of 423 K (bottom red curve). The spectrum of the multilayer shows two peaks centered by Gaussian fitting at 533.4 and 531.7 eV, which based on previous literature are assigned to the oxygen atoms in the hydroxyl (—C—OH) and the carbonyl groups (—C=O), respectively.[23,48] The TDA submonolayer only presents a peak at 531.5 eV, which is associated with two chemically identical oxygen atoms in the carboxylate moieties, reflecting the full deprotonation of the TDA species on Cu(111) at 423 K. Upon deposition of Gd this peak shifts 0.1 eV to a lower binding energy of 531.4 eV. These results are consistent with recently reported Cs-BPyDA[23] and Na-TPA[25] supramolecular architectures on Cu(100), in which a predominant ionic character of the metal–organic bond is claimed, and differ from the metal–organic bond in Fe-carboxylate architectures,[20,48] where coordination interactions are operative.[23]

Figure 4b presents the Gd 3d XPS spectrum for the Gd-TDA supramolecular architecture (same experiment as the one addressed in Figure 4a). The spectrum shows two peaks and two shake-up satellites (with broadness typical of lanthanide systems): the Gd $3d_{3/2}$ at 1218.9 eV and the Gd $3d_{5/2}$ at 1187.4 eV, in agreement to in situ grown gadolinium oxide (cf. Figure SI5, Supporting Information). A comparison to literature results reveals that the binding energy of the Gd $3d_{5/2}$ peak is distinct from metallic Gd (zero oxidation state, 1186.0 eV), coming close to compounds with Gd in a +3 oxidation state (1187.6–1189.1 eV).[49–52]

Further insights into the electronic structure of the coupling motif are provided by an additional evaluation of our DFT results. First, the Bader analysis shows a positive charge of +2.1e for Gd and a negative charge of –1.1e for each of the eight surrounding oxygen atoms involved in the node, which results in a total charge of –0.89e for the metal–organic assembly. Thus, both XPS and DFT results indicate cationic Gd centers in the metallosupramolecular layers.[23] Second, we analyze the electron density displacement field[40] of the Gd-TPA_4 adlayer (cf. **Figure 5**). The field reveals black depletion zones around the Gd center, indicating a strong ionic component in the Gd-TPA_4 coordinative scheme, similar to the Cs-$TCNQ_4$ system, where ionic interactions were deduced.[40]

3. Conclusions

In summary, we have presented a multitechnique study combining low-temperature STM, variable-temperature STM, XPS experiments, and DFT simulations demonstrating the gadolinium-directed assembly of 2D coordination networks on Cu(111) by exploiting metal–ligand interactions between deprotonated TDA linkers and gadolinium centers.

Our data and analysis give insights into the detailed geometry and electronic nature of the lanthanide-carboxylate bond on metallic surfaces, notably indicating chelating arrangements with ionic characteristics. Thanks to the unprecedented coordination number of 8 for the Gd vertexes and the bonding strength, the assemblies are thermally robust. Taking into account the feasibility of incorporating distinct lanthanide elements in similar coordination environments,[36] our

DOI: 10.1002/smll.201502761

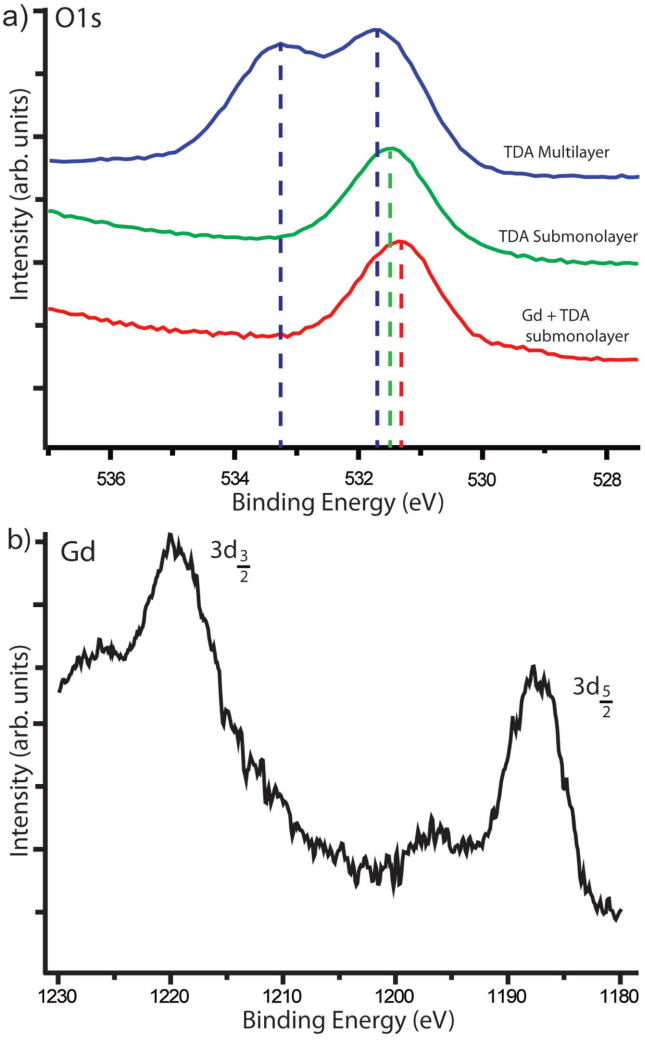

Figure 4. XPS data of TDA molecular species and Gd. a) Oxygen 1s spectra of TDA compounds in three different experiments: TDA multilayer, TDA submonolayer, and mixture of gadolinium atoms and TDA monomers. Vertical dashed lines highlight the shift exhibited by the O1s core level in the different chemical environments. b) Gadolinium 3d background-subtracted photoemission spectrum for Gd atoms deposited on a TDA submonolayer held at 423 K.

study opens novel avenues toward manifold robust rare-earth-carboxylate nanoarchitectures featuring specific functionalities provided from the selected lanthanide and linkers.

4. Experimental Section

Ultrahigh Vacuum Experiments: The experiments were carried out in two distinct custom designed ultrahigh vacuum systems, where the base pressure was below 5×10^{-10} mbar. Measurements at cryogenic conditions (≈6 K) were performed in an ultrahigh vacuum system that hosts a Createc LT-STM. Variable-temperature STM (77–393 K) using an Aarhus-150 STM and XPS investigations were carried out in a unique ultrahigh-vacuum system to allow precise control of surface composition. All STM images were taken in constant-current mode with electrochemically etched tungsten tips, applying a bias (V_{bias}) to the sample. The XPS spectra were

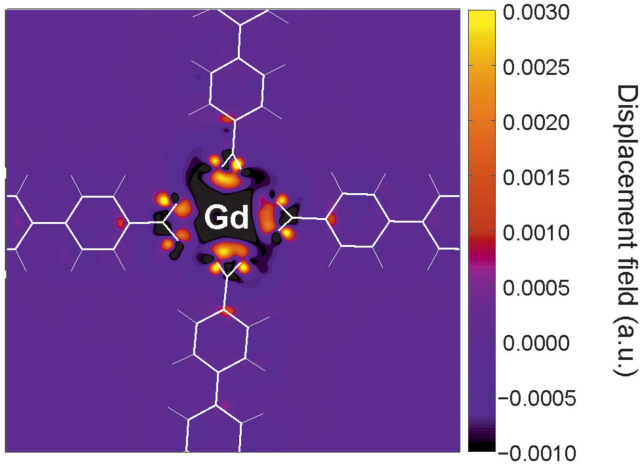

Figure 5. Charge-density displacement field of the Gd-TPA_4 node on the Cu(111) surface. The plot illustrates the difference between electron charge density of the interacting system and those of its noninteracting components. Negative values (violet, black) represent charge depletion, accounting for an ionic character of the Gd center. Positive values (yellow, orange, red) indicate charge accumulation, highlighting the charge gained by the carboxylate moieties. The structure model is superimposed.

recorded utilizing Al Kα X-rays of 1486.6 eV, a FOCUS 500 monochromator, and a PHOBIOS 150 hemispherical electron energy analyzer. The Cu(111) substrate was prepared by standard cycles of Ar+ sputtering (800 eV) and subsequent annealing to 723 K for 10 min. The metal–organic architectures were fabricated following a two-step protocol. First, a submonolayer TDA coverage was prepared by organic molecular-beam epitaxy (OMBE) from a quartz crucible held at 543 K onto a clean Cu(111) crystal at room temperature if not stated otherwise. Subsequently, sample was annealed to 423 K and gadolinium (Gd) atoms were sublimated by means of electron beam evaporation from an outgassed Gd rod (99.9%, MaTecK GmbH, 52428 Jülich, Germany).

Simulations: First-principles calculations have been performed using the VASP package.[53–55] The generalized gradient approximation (GGA) for the exchange-correlation functional of Perdew–Burke–Ernzerhof (PBE)[56] is employed, with dispersion correction using Grimme's DFT-D2 scheme.[57] The effective potentials of core electrons are described using the projector-augmented wave (PAW) pseudopotentials,[58,59] as implemented in the VASP code. For Gd, the valency of the pseudopotential is 9 and the spatially localized 4f electrons are kept frozen in the core. A cutoff energy of 450 eV for the plane wave expansion and a Methfessel–Paxton smearing[60] of 0.2 eV for the occupation of electronic states are chosen. Geometries are optimized with Γ-point for Brillouin-zone sampling until all forces are smaller than 0.02 eV $Å^{-1}$. Single-point energies are calculated with a $3 \times 3 \times 1$ *k*-point mesh according to the Monkhorst–Pack grid.[61] Atomic charges are computed by Bader's topological analysis of the electron density (including the core charge)[62] using the Bader analysis program[63] for VASP. The Cu(111) surface is modeled by a four-layer slab separated by ≈11 Å of vacuum in the surface normal direction, and the topmost two layers are allowed to relax during geometry optimizations. The binding energies are calculated by directly removing the molecule in question from the network whose geometry remains unchanged. In order to visualize

DOI: 10.1002/smll.201502761

the charge transfer in the Gd-TDA adlayer in a 2D presentation, the distribution of the so-called electron density displacement field, DF(x,y), is plotted. The electron density difference ($\Delta\rho$) between the combined system ($\rho_{Gd\text{-}TDA/Cu}$) and the sum of its separated constituents (calculated as freestanding neutral species in the frozen geometry) is defined as $\Delta\rho = \rho_{Gd\text{-}TDA/Cu} - (\rho_{Gd} + \rho_{TDA} + \rho_{Cu})$. DF($x$,$y$) is calculated by integrating $\Delta\rho$ from the plane dividing the substrate and adlayer (z_{sub}) up to vacuum[40]

$$DF(x,y) = \int_{Zsub}^{vacuum} \Delta\rho(x,y,z)dz.$$

Supporting Information

Supporting Information is available from the Wiley Online Library or from the author.

Acknowledgements

J. I. Urgel and B. Cirera contributed equally to this work. Work was supported by the European Research Council Advanced Grant MolArt (Grant No. 247299), the Munich Center for Advanced Photonics (MAP), the Technische Universität München-Institute for Advanced Study, funded by the German Research Foundation (DFG) via the German Excellence Initiative, and by the Comunidad Autónoma de Madrid (CAM) through project No. S2013/MIT-3007 (MAD2D). D.E. thanks funding through the European Marie Curie Program COFUND project No. 291803 (AMARAOUT II) and the Spanish MINECO project RYC-2012-11133. The authors acknowledge allocation of computer time at the Centro de Computación Científica at the Universidad Autónoma de Madrid (CCC-UAM). Y.W., M.A., F.M. thank support by the Spanish MICINN projects FIS2013–42002-R and CTQ2013–43698-P, the CAM project NANOFRONTMAG-CM ref. S2013/MIT-2850, and the European COST Action CM1204 XLIC. W. A. acknowledges funding by the DFG via a Heisenberg professorship.

[1] S. Cotton, *Lanthanide and Actinide Chemistry*, John Wiley & Sons, Chichester (England, UK), **2006**.
[2] J.-C. G. Bünzli, *Acc. Chem. Res.* **2006**, *39*, 53.
[3] S. V. Eliseeva, J.-C. G. Bünzli, *New J. Chem.* **2011**, *35*, 1165.
[4] J.-C. G. Bünzli, *J. Coord. Chem.* **2014**, *67*, 3706.
[5] T. M. Reineke, M. Eddaoudi, M. Fehr, D. Kelley, O. M. Yaghi, *J. Am. Chem. Soc.* **1999**, *121*, 1651.
[6] L. Pan, K. M. Adams, H. E. Hernandez, X. Wang, C. Zheng, Y. Hattori, K. Kaneko, *J. Am. Chem. Soc.* **2003**, *125*, 3062.
[7] C. Qin, X.-L. Wang, E.-B. Wang, Z.-M. Su, *Inorg. Chem.* **2005**, *44*, 7122.
[8] D.-L. Long, A. J. Blake, N. R. Champness, C. Wilson, M. Schröder, *J. Am. Chem. Soc.* **2001**, *123*, 3401.
[9] D.-L. Long, R. J. Hill, A. J. Blake, N. R. Champness, P. Hubberstey, D. M. Proserpio, C. Wilson, M. Schröder, *Angew. Chem. Int. Ed.* **2004**, *43*, 1851.
[10] K. L. Wong, G. L. Law, Y. Y. Yang, W. T. Wong, *Adv. Mater.* **2006**, *18*, 1051.
[11] D.-L. Long, A. J. Blake, N. R. Champness, C. Wilson, M. Schröder, *Angew. Chem. Int. Ed.* **2001**, *40*, 2443.
[12] N. Lin, S. Stepanow, M. Ruben, J. V. Barth, *Top. Curr. Chem.* **2009**, *287*, 1.
[13] H. Liang, Y. He, Y. Ye, X. Xu, F. Cheng, W. Sun, X. Shao, Y. Wang, J. Li, K. Wu, *Coord. Chem. Rev.* **2009**, *253*, 2959.
[14] N. Lin, A. Dmitriev, J. Weckesser, J. V. Barth, K. Kern, *Angew. Chem. Int. Ed.* **2002**, *41*, 4779.
[15] P. Messina, A. Dmitriev, N. Lin, H. Spillmann, M. Abel, J. V. Barth, K. Kern, *J. Am. Chem. Soc.* **2002**, *124*, 14000.
[16] A. Dmitriev, H. Spillmann, N. Lin, J. V. Barth, K. Kern, *Angew. Chem. Int. Ed.* **2003**, *41*, 2670.
[17] S. Stepanow, M. Lingenfelder, A. Dmitriev, H. Spillmann, E. Delvigne, N. Lin, X. Deng, C. Cai, J. V. Barth, K. Kern, *Nat. Mater.* **2004**, *3*, 229.
[18] S. Stepanow, N. Lin, F. Vidal, A. Landa, M. Ruben, J. V. Barth, K. Kern, *Nano Lett.* **2005**, *5*, 901.
[19] U. Schlickum, R. Decker, F. Klappenberger, G. Zopellaro, S. Klyatskaya, M. Ruben, I. Silanes, A. Arnau, K. Kern, H. Brune, J. V. Barth, *Nano Lett.* **2007**, *7*, 3813.
[20] S. L. Tait, Y. Wang, G. Costantini, N. Lin, A. Baraldi, F. Esch, L. Petaccia, S. Lizzit, K. Kern, *J. Am. Chem. Soc.* **2008**, *130*, 2108.
[21] D. Kühne, F. Klappenberger, R. Decker, U. Schlickum, H. Brune, S. Klyatskaya, M. Ruben, J. V. Barth, *J. Am. Chem. Soc.* **2009**, *131*, 3881.
[22] D. Heim, D. Ecija, K. Seufert, W. Auwärter, C. Aurisicchio, C. Fabbro, D. Bonifazi, J. V. Barth, *J. Am. Chem. Soc.* **2010**, *132*, 6783.
[23] S. Stepanow, R. Ohmann, F. Leroy, N. Lin, T. Strunskus, C. Woll, K. Kern, *ACS Nano* **2010**, *4*, 1813.
[24] S. Haq, F. Hanke, M. S. Dyer, M. Persson, P. Iavicoli, D. B. Amabilino, R. Raval, *J. Am. Chem. Soc.* **2011**, *133*, 12031.
[25] D. Skomski, S. Abb, S. L. Tait, *J. Am. Chem. Soc.* **2012**, *134*, 14165.
[26] D. Ecija, S. Vijayaraghavan, W. Auwärter, S. Joshi, K. Seufert, C. Aurisicchio, D. Bonifazi, J. V. Barth, *ACS Nano* **2012**, *6*, 4258.
[27] Y. Li, J. Xiao, T. E. Shubina, M. Chen, Z. Shi, M. Schmid, H.-P. Steinrück, J. M. Gottfried, N. Lin, *J. Am. Chem. Soc.* **2012**, *134*, 6401.
[28] C. S. Kley, J. Čechal, T. Kumagai, F. Schramm, M. Ruben, S. Stepanow, K. Kern, *J. Am. Chem. Soc.* **2012**, *134*, 6072.
[29] L. Wang, H. Kong, C. Zhang, Q. Sun, L. Cai, Q. Tan, F. Besenbacher, W. Xu, *ACS Nano* **2014**, *8*, 11799.
[30] D. Skomski, C. D. Tempas, K. A. Smith, S. L. Tait, *J. Am. Chem. Soc.* **2014**, *136*, 9862.
[31] W. Xu, Q. Tan, M. Yu, Q. Sun, H. Kong, E. Laegsgaard, I. Stensgaard, J. Kjems, J.-G. Wang, C. Wang, F. Besenbacher, *Chem. Commun.* **2013**, *49*, 7210.
[32] H. Kong, L. Wang, Q. Tan, C. Zhang, Q. Sun, W. Xu, *Chem. Commun.* **2014**, *50*, 3242.
[33] T. Lin, G. Kuang, W. Wang, N. Lin, *ACS Nano* **2014**, *8*, 8310.
[34] D. Écija, J. I. Urgel, A. C. Papageorgiou, S. Joshi, W. Auwärter, A. P. Seitsonen, S. Klyatskaya, M. Ruben, S. Fischer, S. Vijayaraghavan, J. Reichert, J. V. Barth, *Proc. Natl. Acad. Sci. USA* **2013**, *110*, 6678.
[35] J. I. Urgel, D. Ecija, W. Auwärter, J. V. Barth, *Nano Lett.* **2014**, *14*, 1369.
[36] J. I. Urgel, D. Ecija, W. Auwärter, A. C. Papageorgiou, A. P. Seitsonen, S. Vijayaraghavan, S. Joshi, S. Fischer, J. Reichert, J. V. Barth, *J. Phys. Chem. C* **2014**, *118*, 12908.
[37] A. Dmitriev, N. Lin, J. Weckesser, J. V. Barth, K. Kern, *J. Phys. Chem. B* **2002**, *106*, 6907.
[38] S. Stepanow, N. Lin, J. V. Barth, K. Kern, *J. Phys. Chem. B* **2006**, *110*, 23472.
[39] D. Grumelli, B. Wurster, S. Stepanow, K. Kern, *Nat. Commun.* **2013**, *4*, 2904.
[40] N. Abdurakhmanova, A. Floris, T.-C. Tseng, A. Comisso, S. Stepanow, A. De Vita, K. Kern, *Nat. Commun.* **2012**, *3*, 940.
[41] A. Floris, A. Comisso, A. De Vita, *ACS Nano* **2013**, *7*, 8059.
[42] S. Clair, S. Pons, A. P. Seitsonen, H. Brune, K. Kern, J. V. Barth, *J. Phys. Chem. B* **2004**, *108*, 14585.
[43] J. V. Barth, J. Weckesser, N. Lin, A. Dmitriev, K. Kern, *Appl. Phys. A* **2003**, *76*, 645.

DOI: 10.1002/smll.201502761

[44] A. P. Seitsonen, M. Lingenfelder, H. Spillmann, A. Dmitriev, S. Stepanow, N. Lin, K. Kern, J. V. Barth, *J. Am. Chem. Soc.* **2006**, *126*, 5634.
[45] S. Clair, S. Pons, S. Fabris, S. Baroni, H. Brune, K. Kern, J. V. Barth, *J. Phys. Chem. B* **2006**, *110*, 5627.
[46] Y. Han, X. Li, L. Li, C. Ma, Z. Shen, Y. Song, X. You, *Inorg. Chem.* **2010**, *49*, 10781.
[47] H. Spillmann, A. Dmitriev, N. Lin, P. Messina, J. V. Barth, K. Kern, *J. Am. Chem. Soc.* **2003**, *125*, 10725.
[48] S. Stepanow, T. Strunskus, M. Lingenfelder, A. Dmitriev, H. Spillmann, N. Lin, J. V. Barth, C. Wöll, K. Kern, *J. Phys. Chem. B* **2004**, *108*, 19392.
[49] J. F. Moulder, W. F. Stickle, P. E. Sobol, K. D. Bomben, *Handbook of X-Ray Photoelectron Spectroscopy*, Physical Electronics Division (Perkin-Elmer Corporation), Eden Prairie (Minnesotta, USA), **1992**.
[50] C. J. Powell, A. Jablonski, *NIST Electron Effective-Attenuation-Length Database-Version 1.3*, National Institute of Standards and Technology, **2011**.
[51] D. Raiser, J. P. Deville, *J. Electron Spectrosc.* **1991**, *57*, 91.
[52] G. Ebbinghaus, A. Simon, A. Griffith, *Z. Naturforsch.* **1982**, *37a*, 564.
[53] G. Kresse, J. Hafner, *Phys. Rev. B* **1994**, *49*, 14251.
[54] G. Kresse, J. Furthmüller, *Phys. Rev. B* **1996**, *54*, 11169.
[55] G. Kresse, J. Furthmüller, *Comput. Mater. Sci.* **1996**, *6*, 15.
[56] J. P. Perdew, W. Burke, M. Ernzerhof, *Phys. Rev. Lett.* **1996**, *77*, 3965.
[57] S. Grimme, *J. Comp. Chem.* **2006**, *27*, 1787.
[58] P. E. Blöchl, *Phys. Rev. B* **1994**, *59*, 17953.
[59] G. Kresse, D. Joubert, *Phys. Rev. B* **1999**, *59*, 1758.
[60] M. Methfessel, A. Paxton, *Phys. Rev. B* **1989**, *40*, 3616.
[61] H. J. Monkhorst, J. D. Pack, *Phys. Rev. B* **1976**, *13*, 5188.
[62] R. F. W. Bader, *Atoms in Molecules – A Quantum Theory*, Oxford University Press, London **1990**.
[63] A. Arnaldsson, W. Tang, G. Henkelman, Bader analysis program, http://theory.cm.utexas.edu/henkelman/code/bader (accessed: October, 2015).

Received: September 11, 2015
Revised: September 25, 2015
Published online: